Force-enhanced atomic refinement: Structural modeling with interatomic forces in a reverse Monte Carlo approach applied to amorphous Si and SiO_{2}

A. Pandey, Parthapratim Biswas, and D. A. Drabold

Force Enhanced Structural Refinement (FESR): A novel approach to structural modeling

A. Pandey,[1] Parthapratim Biswas,[2] and D. A. Drabold[3]

[1]*Department of Physics and Astronomy, Condensed Matter and*
Surface Science Program, Ohio University, Athens OH 45701, USA
[2]*Department of Physics and Astronomy, The University of Southern Mississippi, Hattiesburg MS 39406, USA*
[3]*Department of Physics and Astronomy, Ohio University, Athens OH 45701, USA*
(Dated: October 12, 2015)

We introduce a novel structural modeling technique: Force Enhanced Structural Refinement (FESR). The technique incorporates interatomic forces in Reverse Monte Carlo (RMC) simulations for structural refinement by fitting experimental diffraction data using the conventional RMC algorithm, and minimizes the total-energy and forces from an interatomic potential. We illustrate the usefulness of the approach by studying a-SiO$_2$ and a-Si. The structural and electronic properties of the FESR models agree well with experimental neutron and x-ray diffraction data, and the results obtained from previous molecular-dynamics simulations of a-SiO$_2$ and a-Si. We have shown that the method is more efficient than the conventional molecular-dynamics simulations via 'melt-quench'. The computational time in FESR has been observed to scale quadratically with the number of atoms.

I. INTRODUCTION

An ideal approach to computational modeling of complex amorphous materials should incorporate the state-of-the-art total-energy and force methods and the judicious application of *a priori* information–experimental data pertaining to the material. When these schemes are suitably merged, the resulting structural models should reflect our full state of knowledge about the material. Conventional molecular-dynamics (MD) simulations of amorphous materials suffer from several difficulties. Most serious of all is the high computational cost associated with simulating large models using quantum-mechanical methods, such as *ab initio* molecular dynamics (AIMD) based on the density-functional theory. Further, for amorphous solids with *weak* or no *glassy* behavior (e.g. *a*-Si and *a*-Ge), AIMD performs poorly that requires development of new approaches to address these materials. Similarly, computational approaches that attempt to construct structural models of amorphous solids by inverting experimental data, along with the local chemical and geometrical ordering of the networks, often fail. Such *inverse* approaches crucially rely not only on the quality and availability of experimental information but also on the ability of the approaches to effectively include *a priori* information in simulations. An archetypal example is the Reverse Monte Carlo (RMC) method[1,2], which constructs a three-dimensional model of a material by inverting experimental diffraction data. While RMC is very simple to implement and has been used to model a variety of disordered solids[3–5] (e.g. glasses, liquids, polymers, etc.) in the past, the very scalar nature of diffraction data dictates that the method cannot be used to uniquely determine the structure of amorphous solids using diffraction data only. This has led to the development of a number of hybrid approaches that successfully couple a total-energy functional (quantum-mechanical or otherwise) with *a priori* information. To this end, the purpose of this paper is to present a hybrid approach that effectively imposes *a priori* information on a simulation process.

Logically, one should include as much *a priori* information as possible from experimental data, as well as from chemical and geometrical knowledge of the material, to produce structures consistent with experiments[6]. Compelling 'uniformity' as a constraint, for the refinement of the atomistic-scale structures, was adopted by Goodwin and coworkers in their INVERT technique[7]. A liquid-quench procedure, combined with a hybrid Reverse Monte Carlo (HRMC) approach, which incorporates both experimental and energy-based constraints has been employed by Opletal and coworkers in their study of amorphous carbon[8]. A similar approach via HRMC with bonded and non-bonded forces was used by Gereben and Pusztai to study liquid dimethyl trisulfide[9]. Likewise, by refining the initial interatomic empirical potential-energy function and fitting the input experimental structure-factor data, empirical potential structure refinement (EPSR) has been quite successful in predicting liquid structures[10]. An alternative approach, experimentally constrained molecular relaxations (ECMR), which incorporates experimental information in first-principles modeling of materials in a 'self-consistent' manner was discussed in[11]. The approach presented in this paper provides an alternative scheme to develop a self-consistent implementation of the ECMR with a minimal computational overhead. Recently, a means for including *electronic a priori* information has also appeared[12].

In this paper, we report a novel structural modeling technique: Force Enhanced Structural Refinement (FESR). To test the effectiveness of this approach, we have conducted structural modeling of a-SiO$_2$ and a-Si. Our method uses RMC to fit the input experimental data and parsimoniously employs interatomic forces obtained from (classical)

total-energy functionals to restrict the search in the energetically-favorable region of the configuration space in a self-consistent manner. Unlike other hybrid approaches[8,9], where the total-energy of the system is coupled to RMC for accepting and rejecting atomic moves, the movement of the atoms in FESR, due to interatomic forces, is independent of the RMC moves. This enhances the efficiency of the method by reducing the total computational cost associated with force calls. The computational efficiency of the technique has been studied by comparing the number of force calls with other MD approaches.

The rest of this paper is organized as follows. In section II, we describe the basics of the FESR method and its implementation. Section III discusses the results for a-SiO_2 and a-Si. In section IV, we present the conclusions of our work.

II.   METHODOLOGY: BASICS OF FESR AND ITS IMPLEMENTATION

A review of Reverse Monte Carlo (RMC)[1,3,4,8,11] and the related methods suggests that diffraction data alone is insufficient to determine the structure of complex amorphous solids. This is particularly so for amorphous semi-conductors, where the presence of directional bonding cannot be inferred directly from one-dimensional diffraction data only. While the inclusion of structural constraints proves to be particularly useful in RMC simulations[13], they do introduce additional complexities in the search space. For multi-component systems, this can be a serious impediment and, in some cases, may render the problem intractable even with gradient information. The choice of appropriate constraints itself can be highly nontrivial. Owing to the hierarchical nature of the geometrical/structural constraints in complex disordered systems, it is generally beneficial to include lower-order constraints first, which are followed by higher-order constraints of increasing complexity and information content. However, the presence of too many constraints can be detrimental to a problem due to the competition between the constraints. Such competing constraints can adversely affect the efficiency of a search procedure by introducing complex rugged structure in the multi-dimensional configuration space, which makes it difficult for the optimizer to evolve and, thus, to determine the optimal solution space for structural determination. Further, the correct structural solutions often crucially depend on the strength of the constraints (i.e. weight factors), which are generally obtained heuristically after several trial runs in optimizations based on stochastic search algorithms. Thus, the determination of structure of complex disordered solids from a set of experimental data and structural/geometrical constraints continues to pose a challenging problem in condensed-matter sciences.

In the present approach, we intend to avoid some of these difficulties by introducing the following steps: i) optimization of a total-energy and penalty functionals in separate subspace; ii) inclusion of gradient information to optimize the total-energy functional; iii) incorporation of special atomic displacements to enhance the convergence of total energy during subspace optimization by moving a set of atoms associated with strained local configurations. Step I essentially eliminates the need for weight factors that are necessary for optimization of an augmented 'effective energy' functional. Instead, subspace optimizations proceed in tandem with each other and, thereby, establish a 'coupling' between steps I and II. Unfavorable configurations, which are generated in step I, are either corrected or rejected in step II and vice versa. We emphasize that the approach is highly flexible; the exact implementation of the method can vary and may depend on the degree of accuracy and the efficiency one needs to achieve in optimizing models with several hundreds atoms. While a number of sophisticated algorithms can be employed for subspace optimizations (such as deterministic conjugate-gradient[14] type approaches to stochastic exchange-replica Monte Carlo[15] and evolutionary search procedures[16]), for the sake of simplicity and exploring the efficacy of this approach at its basic level, we confine ourselves to the steepest-descent method and Reverse Monte Carlo approach for optimizing the total energy and experimental structure-factor data, respectively. We show that even at this elementary level of implementation, the method is profitable and holds the promise for further development using the state-of-the-art multi-objective optimization (MOO) techniques developed in recent years. Thus, in the FESR approach, the statement of the problem can be written as:

$$\min_{\{q\}} P(\{q\}), \quad P \equiv \chi^2 \otimes \Phi, \tag{1}$$

where Φ, χ^2, and $\{q\}$ stand for a total-energy functional, a penalty function involving experimental structure factor, and 3N-dimensional configurational coordinates, respectively. Following McGreevy and others[1,5], we can write,

$$\chi^2 = \sum_i \left[\frac{F_E(k_i) - F_C(k_i)}{\sigma(k_i)} \right]^2, \tag{2}$$

where $F_{E/C}(k_i)$ is the experimental/computational structure factor, and $\sigma(k_i)$ is the error associated with the experimental data for wave vector k_i.

To illustrate our method, we have chosen two canonical examples of amorphous systems: amorphous silica (a-SiO$_2$) and amorphous silicon (a-Si). The former is a classic glass-former, and can be readily obtained by quenching molten models at high temperature. The latter is preferably modeled via event-based approaches, such as Winer-Wooten-Weire (WWW)[17] and activation-relaxation techniques[18]. Both systems have been studied extensively in the literature, which provides a wealth of information for comparing experimental data with computational results for various physical quantities. Here, we choose to employ the environment-dependent interatomic potential (EDIP) by Justo et al.[19] for modeling a-Si. For a-SiO$_2$, we choose the potential proposed by Beest et al. (BKS) and their parameters[20]. The functional form of the BKS potential is given by,

$$\phi_{i\alpha,j\beta} = \frac{Q_\alpha Q_\beta}{r_{i\alpha,j\beta}} + A_{\alpha\beta}\exp(-B_{\alpha\beta}\,r_{i\alpha,j\beta}) - \frac{C_{\alpha\beta}}{r_{i\alpha,j\beta}^6}, \tag{3}$$

where $\phi_{i\alpha,j\beta}$ is the interaction energy between two atoms of species α and β at sites i and j, respectively. The parameters Q, A, B and C depend on atomic species and can be found in [21].

The presence of the electrostatic interaction in Eq. 3 stipulates that the Ewald summation [22] should be used in the calculation of the total energy and forces. However, as shown by Wolf et al. [23] in a recent communication, a pairwise sum can be constructed in real space by ensuring charge neutrality of the system such that the sum produces results very similar to that obtained from the Ewald summation. We have adopted this real-space approach to calculate the total energy and forces via Wolf's summation. Following these authors, the expression for the electrostatic force between two species α and β at sites i and j can be written as:

$$F^{i\alpha,j\beta} = Q_\alpha Q_\beta \left\{ \frac{\mathrm{erfc}(\kappa r_{i\alpha,j\beta})}{r_{i\alpha,j\beta}^2} + \frac{2\kappa}{\pi^{1/2}} \frac{\exp(-\kappa^2 r_{i\alpha,j\beta}^2)}{r_{i\alpha,j\beta}} \right.$$
$$\left. - \frac{\mathrm{erfc}(\kappa R_c)}{R_c^2} - \frac{2\kappa}{\pi^{1/2}} \frac{\exp(-\kappa^2 R_c^2)}{R_c} \right\}, \quad \text{for} \ \ r_{i\alpha,j\beta} \le R_c. \tag{4}$$

The damping coefficient (κ) and the cutoff radius (R_c) play an important role in the calculation by including contributions from the reciprocal and real spaces. Since these parameters are not independent of each other, care must be taken to choose an appropriate set of values for accurate calculations of total energy and forces. Following Fennell and Gezelter[24], we have used a value of 0.2 and 9 Å for κ and R_c, respectively.

Figure 1 presents a schematic diagram of the FESR method showing the principal steps of our calculations. Starting with an initial random configuration $\mathbb{C}_1$, the method proceeds via χ^2 minimization to generate a new configuration $\mathbb{C}_2$ by enforcing experimental structure factor using conventional Reverse Monte Carlo (RMC) simulations. The output from this step is then fed to the next step for optimization of total energy via a gradient-descent approach. The structure of the resulting configuration $\mathbb{C}_3$ is then examined for continuation or termination. This self-consistent iterative scheme continues until the convergence criteria for each subspace optimization are met or a maximum number of iteration is reached. The total-energy optimization and the χ^2-fitting of the structure factor constitute the principal components of the method, and are indicated in Fig. 1 by the loop: $2 \to 3 \to 4 \to 2$. In the next section, we apply this method to a-SiO$_2$ and a-Si, and discuss the results in details.

III. RESULTS AND DISCUSSION

A. Amorphous silica (a-SiO$_2$)

In this subsection, we present results for a-SiO$_2$ from FESR simulations. To this end, we use total neutron static structure factor from[6] which is then coupled with the total-energy BKS functional to generate a-SiO$_2$ models consisting of 192, 648, 1020 and 1536 atoms. Starting with a random configuration with an experimental density of 2.20 $g\,cm^{-3}$ for a-SiO$_2$, the structure factor of the model is fitted with the corresponding experimental data via RMC simulations. After 100 successful RMC moves, the total energy and forces on the atoms are calculated (using a single force call) and the atoms are displaced along the direction of forces. This 2-step process is then repeated until the convergence criteria for χ^2 and the total energy are satisfied. Analysis of χ^2 and total energy suggest that approximately 3×10^4 force calls are sufficient for FESR to converge to a reasonable accuracy of $\delta\chi^2 \approx 10^{-4}$ and $\delta F \approx 0.02$ eV/Å for system sizes we have studied so far.

To estimate the overall computational cost of the method, we have calculated the total CPU time for several system sizes, and compared the results with those obtained from classical and *ab initio* MD simulations reported in[25,26]. In Fig.2, we have plotted the CPU time for $N = 192$, 648, 1020 and 1536 atoms. While both RMC and force calculations

can be implemented in an order-N manner (see note[38]), we made no attempts to obtain such improved scaling at this time in an effort to examine the usefulness of this approach in this exploratory study. Thus, the CPU time for a run has been observed to scale quadratically with the system size. This is indicated in Fig. 2 by a least-square fit of the data using a quadratic polynomial. Despite this quadratic scaling of CPU time, a notable feature of the method is the parsimonious use of gradient information for structural optimization. FESR makes significantly fewer force calls than conventional classical/*ab initio* MD or other gradient-based methods. A comparison of the number of force calls relaxation between FESR and melt-quench MD (classical and *ab initio*)[25,26] can be found in Table I.

The partial pair-correlations data for the FESR models are shown in Table II. The peak positions and bond lengths are comparable with the results from other MD models and experiments. The average coordination numbers of Si and O for the model with 1536 atoms are found to be 3.98 and 1.99, respectively. The presence of a few 3-fold (3.2 %) and 5-fold (0.45 %) silicon and isolated (2.7 %) oxygen atoms can be attributed to the BKS potential that lacks the three-body term[20]. None of the FESR models shows any chemical disorder or heteropolar bonding.

The total structure factor $S(k)$ is compared to the neutron diffraction experiments from Ref.[6], and is shown in Fig. 4. The origin of the peaks in $S(k)$ can be inferred from partial structure factors. The second peak in Fig. 4 arises from Si–Si and O–O correlations with a partial cancellation from the Si–O anti-correlations. The third and fourth peaks receive contributions of Si–Si, Si–O and O–O correlations. The first peak for both the models is small compared to the experiment which can be attributed to finite-size effects in the intermediate range order [27].

In Fig. 5, we have shown the variation of the cost function (χ^2) and BKS energy per atom during FESR simulations. The horizontal line in the plot corresponds to the BKS energy for a 648-atom model obtained from the decorate-and-relax approach described elsewhere[29]. The BKS energy, for both 1536- and 648-atom models, is close to -19.15 eV/atom, which is comparable to -19.18 eV/atom from the corresponding DR model. The use of atomic forces or gradient information improves the quality of structure.

The bond-angle distributions for the model with 1536 atoms are plotted in Fig. 6. The distribution of ∠O-Si-O shows that the silicon-centered O-Si-O angles are tetrahedral in character with an average value of 109.5° and a full width (at half maximum) of 15.6°. These values are consistent with the experimental data reported by Mozzi and Warren[30]. The corresponding values for ∠Si-O-Si are found to be 154.3° and 27.8°, respectively. The average value of ∠Si-O-S is about 6.4% higher than the experimental value of 144°, and the value obtained from other theoretical models[25,27]. This deviation, however, is not surprising, and is generally attributed to the lack of 3-body interaction in the BKS potential[31]. Since Si-O-S angles involve two neighboring tetrahedra connected via a bridging oxygen atom at a common vertex, it is difficult for the BKS potential to produce this delicate geometrical arrangement accurately via 2-body interactions only. A full comparison of FESR results with experimental data and other theoretical models are provided in Table III.

Table IV presents the number of irreducible ring statistics for the models with 192, 648, and 1536 atoms using the I.S.A.A.C.S program [32]. The presence of only even-member rings implies the absence of chemical disorder in the network.

The structures obtained from FESR have been relaxed using the density-functional code (VASP) using a local-density approximation (LDA) and the LDA energies have been found to be comparable with those obtained from the DR model[29]. The electronic density of states (EDOS) for a 192-atom a-SiO$_2$ is shown in Fig.7. The EDOS is comparable with the results obtained by Sarnthein and co-workers[26] and hence with the X-ray photoemission spectra (XPS)[33] in the sense that the states are well reproduced. There are three distinct regions of occupied states. The states about -18 eV are oxygen 2s states, while the one between -10 eV and -4 eV are the bonding states between Si sp^3 hybrids and O 2p orbitals. The highest occupied states in valence band about -4 eV are the O 2p states and the lowest unoccupied states of conduction band comprise of anti-bonding states. However, the band gap of 3.96 eV is underestimated compared to 4.8 eV of that obtained from MD calculation[26] and the experimental value of 9.0 eV[34]. This is to be expected from LDA DFT calculations.

Finally, to verify the reproducibility of the method, we have generated 20 configurations of 192- and 648-atom models, and 10 configurations of 1020- and 1536-atom models from different random starting configurations. Approximately, 90% of final configurations have been observed to have almost identical structural and electronic properties. The configuration fluctuations of various physical observables are found to be within the statistical limits, which ensure the reproducibility and consistency of the FESR method.

B. Modeling amorphous silicon (a-Si)

We have also employed FESR to model structure of a-Si starting from a random configuration with 216 atoms. The results of our calculations are plotted in Figs. 8-12. Figure 8 shows the structure factor obtained from a 216-atom FESR model of a-Si along with the experimental X-ray diffraction data from [35]. It is evident from Fig. 8 that the structure factor agrees very well with the experimental data except for a few points near the first peak. This is also

reflected in the correlation data in real space in Fig. 9, where the pair-correlation function of the FESR model is compared with the same from a WWW model.

The cost function χ^2 and the total EDIP energy is shown in Fig. 10. The energy is compared to the 216-atom a-Si WWW model which is 4.199 eV (shown by dashed line). This shows that in FESR, the energy is minimized together with the structural refinement.

The bond-angle distribution is shown in Fig.11a where the tetrahedral geometry is retained compared to the WWW model of identical number of atoms. The corresponding bond-angle distribution using RMC is shown in Fig.11b where the peaks are highly underestimated and the distribution is broad without tetrahedral peak. We relaxed the structure obtained from FESR using VASP and found the energy minimum to be -5.18 eV/atom compared to -5.23 eV/atom of the VASP relaxed WWW model. This shows that the LDA energies are comparable. In Fig.12, the electronic density of states for the FESR model is compared with the same from a VASP-relaxed WWW model. The Fermi energies are shown by the vertical dashed lines. As compared to RMC and constrained RMC[2], the EDOS is in better agreement with optical measurements. The FESR model exhibits the presence of several defect states within the gap, which mostly arise from coordination defects. This is expected in view of the fact that approximately 10% of total Si atoms have a coordination number, which is different from 4. This coordination number is better compared to the constrained RMC (88%)[2] and MD Quench from melt using EDIP and Tersoff potentials[36,37]. The EDIP for Si overestimates the five-fold bond in Si which is evident in our FESR calculation with almost 8% 5-fold Si present in the network[36]. These floating bonds, clutter the gap and form defects states that closes the gap. The presence of these defect states, and the use of the LDA that is known to underestimate the optical gap, explains the small gap in the electronic density of states.

IV.   CONCLUSIONS

In this paper, we have studied a new approach–Force Enhanced Structural Refinement (FESR)–to model complex amorphous solids by combining experimental structure factor with periodic usages of gradient information from a total-energy functional. The approach consists of employing experimental scattering data to generate an ensemble of possible structural solutions via Reverse Monte Carlo simulations, which is followed by further refinement of the RMC solutions using gradient information from a total-energy functional. Since conventional RMC cannot describe a 3-dimensional structure uniquely, and its constrained counterpart with additional structural information often transforms the original unconstrained problem to a difficult multi-objective optimization program, the emphasis on the present approach has been to develop a method that retains the simplicity of RMC and yet overcomes the problem of non-uniqueness in structural determination via the economical use of a total-energy functional and forces. The approach can be viewed as a 'predictor-corrector' method for structural refinement. Atomistic configurations predicted by RMC are corrected at regular interval via the optimal usage of gradient information or forces from a total-energy functional. This enables FESR to track solutions in the manifold of the solution space that jointly satisfies experimental structure-factor data and the total energy of the system. In this exploratory study, we have demonstrated using two archetypal examples of amorphous solids (a-Si and a-SiO$_2$) that the method performs on a par with the traditional MD simulations or other gradient-based relaxation approaches even at an elementary level of its implementation.

We have successfully implemented FESR to model a-SiO$_2$ and a-Si. Structural and electronic properties of the FESR models are produced as accurately as possible within the limit of the potentials and experimental input data. The structural properties of FESR models have been examined by analyzing the pair-correlation data, bond-angle distributions, ring statistics and the distribution of the tetrahedral building blocks of the underlying network structure of a-SiO$_2$ and a-Si. Electronic properties of the models are also studied primarily by calculating the electronic density of states within the density-functional framework using the plane-wave based VASP code using a local-density approximation. A comparison of FESR results with those obtained from ab $initio$ and classical simulations[25,26] are also discussed.

We conclude this section with the following observations. First, the method can be improved further by using efficient algorithms for both RMC and total-energy calculations. The former can be readily implemented using an $O(n)$ algorithm. Similarly, by using more sophisticated algorithms for the minimization of total energy, it is possible to accelerate the convergence of total energy and forces during FESR simulations. Second, the very economical nature of the use of gradient information (or forces) suggests that the method would be particularly useful when employed with ab $initio$ total-energy functionals. Since ab $initio$ calculations of total energy and forces for complex disordered solids (with system size) are almost always proportional to $O(n^3)$, an implementation of FESR within ab $initio$ packages will provide an effective tool for total-energy relaxations. Last but not least, we anticipate, it would be possible to develop a more effective coupling scheme between the solution space (defined by a set of experimental data) and the configuration space (of a total-energy functional) such that a mechanism can be built into FESR to avoid solutions

associated with unphysical or poor structures. In a future communication, we will address some of these issues.

V. ACKNOWLEDGEMENTS

[1] O. Gereben and L. Pusztai, Phys. Rev. B **50**, 14 136 (1994).

[2] P. Biswas, R. Atta-Fynn and D. A. Drabold, Phys. Rev. B **69**, 195207 (2004).

[3] D. A. Keen and M. T. Dove, J. Phys.: Condens. Matter **11** 9263 (1999).

[4] S. Kohara and K. Suzuya, J. Phys.: Condens. Matter **17** S77-S86 (2005).

[5] Mc Greevy R L, J. Phys.: Condens. Matter **13** R 877 (2001).

[6] D. N. Tafen and D. A. Drabold, Phys. Rev. B **71**, 054206 (2005).

[7] M. J. Cliffe, M. T. Dove, D. A. Drabold and A. L. Goodwin, Phys. Rev. Lett. **104**, 125501 (2010).

[8] G. Opetal, T. C. Petersen, D. G. McCulloch, I. K. Snook and I. Yarovsky, J. Phys.: Condens. Matter **17** (2005).

[9] O. Gereben and L. Pusztai, Journal of Computational Chemistry **33** (29), 2285-2291 (2012).

[10] A. K. Soper, Mol. Phys. Vol **99**, No. 17, 1503-1516 (2001).

[11] P. Biswas, D. N. Tafen, R. Atta-Fynn and D. A. Drabold, J. Phys.: Condens. Mattter **16** (2004).

[12] K. Prasai, P. Biswas and D. A. Drabold, Scientific Reports (in press).

[13] P. Biswas, D. N. Tafen, F. Inam, B. Cai and D. A. Drabold, J. Phys.: Condens. Matter **21** 084207 (2009).

[14] J. Nocedal and S.J. Wright, *Numerical Optimization*, Springer Series in Operations Research, Springer 2006.

[15] D. J. Earl and M. W. Deem, Phys. Chem. Chem. Phys., **7**, 3910 (2005).

[16] A. E. Eiben and J. E. Smith, *Introduction to Evolutionary Computing*, Natural Computing Series, Springer 2008.

[17] F. Wooten, K. Winer and D. Weairie, Phys. Rev. Lett. **54**, 1392 (1985).

[18] G. T. Barkema and N. Mousseau, Phys. Rev. Lett. **77**, 4358 (1996).

[19] J. F. Justo, M. Z. Bazant, V. V. Bulatov and S. Yip, Phys. Rev. B **58**, 2539 (1998).

[20] B. W. H. van Beest, G. J. Kramer and R. A. van Santen, Phys. Rev. Lett. **64**, 16 (1990).

[21] A. Carre, J. Horbach, S. Ispas and W. Kob, Eur. Phys. Lett., **82** 17001 (2008).

[22] U. Essmann, L. Perera, M. L. Berkowitz, T. Darden, H. Lee, L. Pedersen, J. Chem. Phys. **103** (19), 8577-8593 (1995).

[23] D. Wolf, P. Keblinski, S.R. Phillpot and J. Eggebrecht, J. Chem. Phys. **110** 17 (1999).

[24] C. J. Fennell and J. D. Gezelter, J. Chem. Phys. **124** 234104 (1999).

[25] P. Vashista, R. K. Kalia and J. P. Rino, Phys. Rev. B **41**, 17 (1990).

[26] J. Sarnthein, A. Pasquarello and R. Car, Phys. Rev. Lett. **74**, 23 (1995).

[27] A. Nakano, R. K. Kalia and P. Vashishta, J. Non-Cryst. Solids **171**, 157-163 (1994).

[28] Q. Mei and C. J. Benmore, Phys. Rev. B **78**, 144204 (2008).

[29] D. N. Tafen and D. A. Drabold, Phys. Rev. B **68**, 165208 (2003).

[30] L. Mozzi and B. E. Warren, J. Appl. Crystallogr. **2**, 164 (1969).

[31] C. Massobrio, J. Du, M. Bernasconi and P. S. Salmon, Springer Series in Materials Science, Vol. **215** (2015).

[32] S. Le Roux and V. Petkov , J. Appl. Crystallogr., **43**: 182-185 (2010).

[33] B. Fischer, R. A. Pollak, T. H. DiStefano and W. D. Grobma, Phys. Rev. B **15**, 3193 (1977).

[34] M. Benoit, S. Ispas, P. Jund and R. Jullien, Eur. Phys. J. B, **13** 631-636 (2000).

[35] K. Laaziri *et al.*, Phys. Rev. Lett. **82**, 3460 (1999).

[36] P. Keblinski, M. Z. Bazant, R. K. Dash and M. M. Treacy, Phys. Rev. B **66**, 064104 (2002).

[37] M. Ishimaru, S. Munetoh and T. Motooka, Phys. Rev. B **56**, 23 (1997).

[38] For *empirical* potentials with a finite cutoff R_c, the number of force evaluation is proportional to pN, where p is the average number of atoms within the interacting sphere of radius R_c and N is the total number of atoms in the system. The list of p atoms can be constructed periodically in an $O(N)$ manner by partitioning the entire volume into several cells, and generating a list of atoms in each cell. The $O(N)$ calculation of pair-correlation data can be achieved in a straightforward way.

Figures
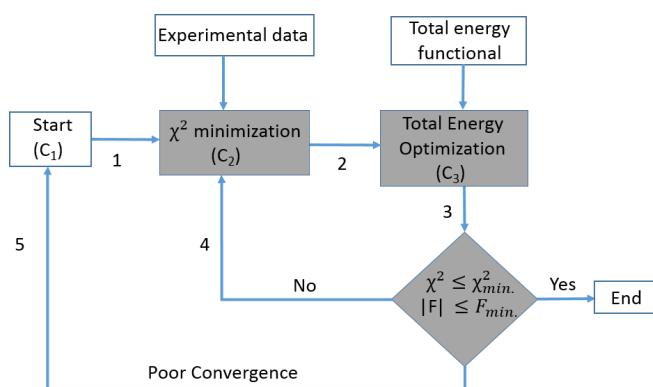
FIG. 1: A schematic diagram of the FESR method. The principal computing loop is highlighted in grey.
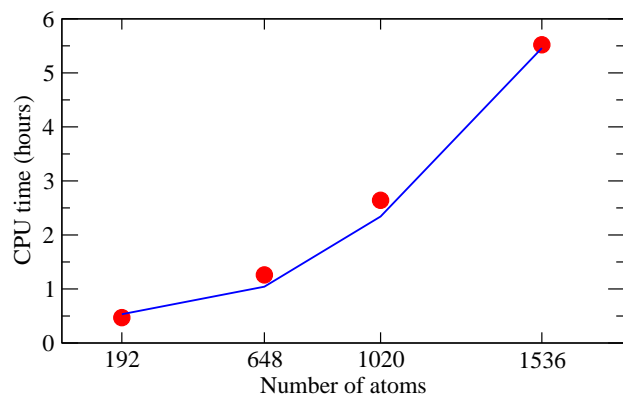
FIG. 2: (Color online) Scaling of total CPU time (red circles) vs. system size in FESR simulations. A least-square fit of the data with a quadratic polynomial is shown as a blue curve.
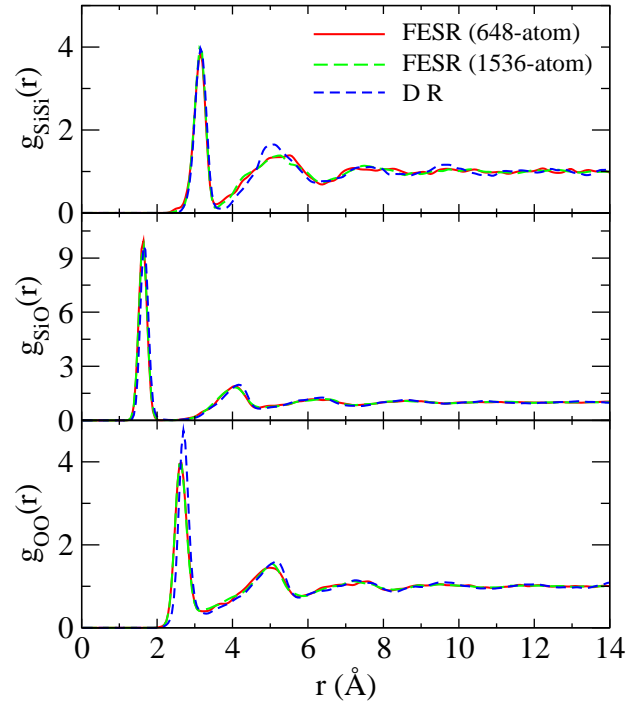
FIG. 3: (Color online) Partial pair-correlation data for a-SiO$_2$ models from FESR simulations. The corresponding data (dashed blue curve) for a DR model from[29] are included for comparison.
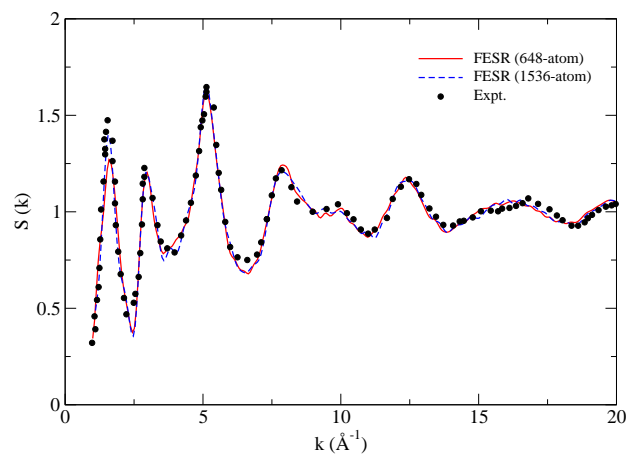
FIG. 4: (Color online) Calculated total neutron static structure factor for 648- and 1536-atom a-SiO$_2$ models from FESR simulations. Experimental data from[6] are shown as solid circles.
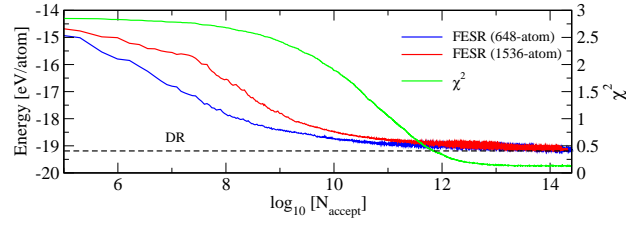
FIG. 5: (Color online) Total energy (of a-SiO$_2$) and the cost function χ^2 vs. RMC steps during FESR simulations. The horizontal line corresponds to the energy of a DR model using the BKS potential for comparison.
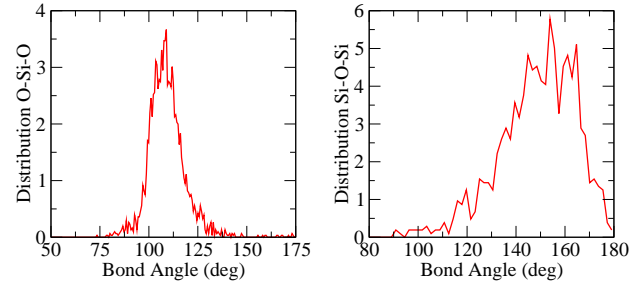
FIG. 6: (Color online) Bond-angle distributions of a 1536-atom model of a-SiO$_2$ from FESR calculations. The average and width of the distributions are listed in Table III.
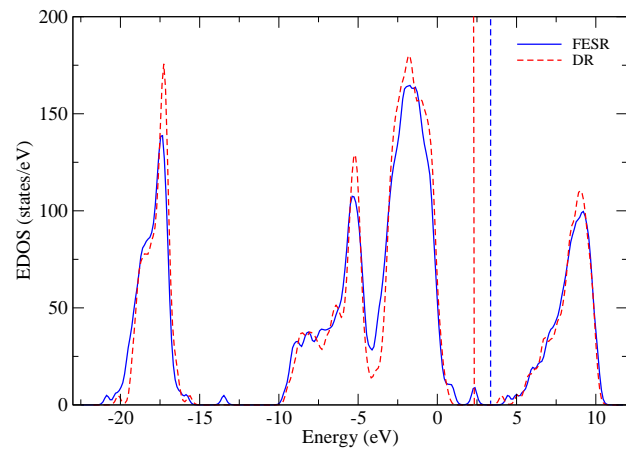
FIG. 7: (Color online) Electronic density of states (EDOS) for a 192-atom model of a-SiO$_2$ obtained from FESR simulations. The corresponding result from a DR model is included for a comparison. Fermi levels are indicated as vertical lines at 2.4 eV (DR) and 3.4 eV (FESR).
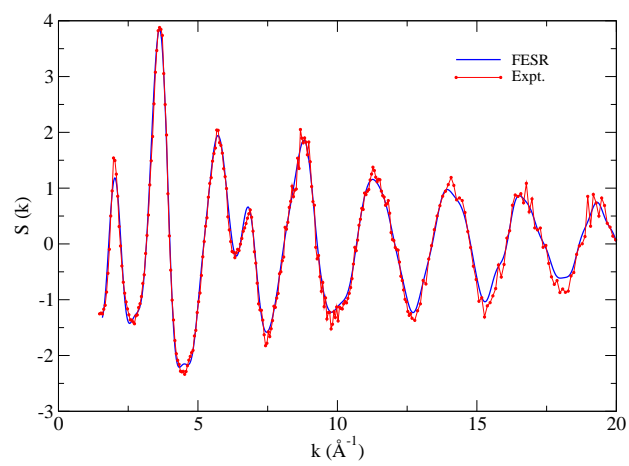
FIG. 8: (Color online) A comparison of FESR structure factor for a 216-atom model of a-Si with the experimental data from Ref. [35].
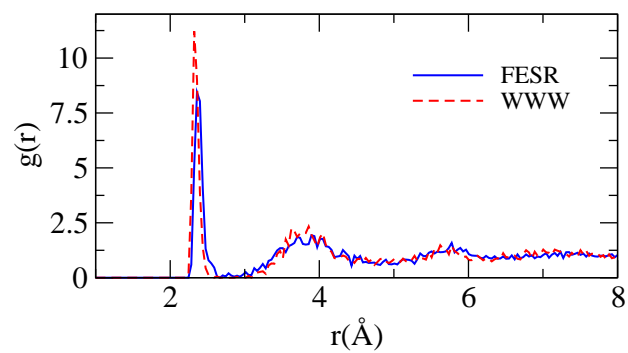
FIG. 9: (Color online) Pair-correlation data (blue) for a 216-atom model of a-Si obtained from FESR. The corresponding data (red) for a WWW model is also presented here for a comparison.
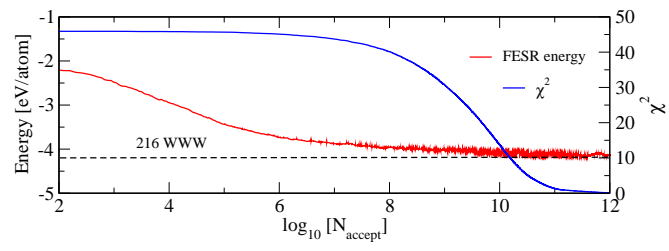
FIG. 10: (Color online) The variation of χ^2 and EDIP energy during FESR simulations. The dashed line is the EDIP energy for a WWW model with an identical size and the number density.
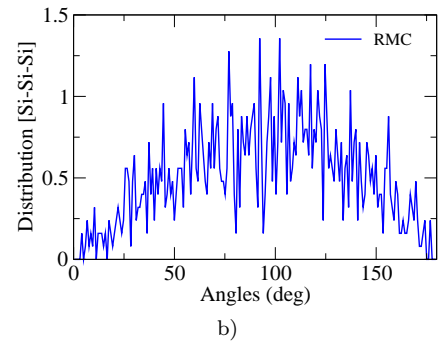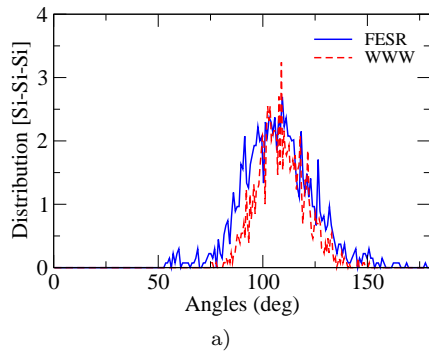
FIG. 11: (Color online) (a) The bond-angle distribution for a 216-atom model of *a*-Si using FESR (solid line) and a WWW model (dashed line). (b) The bond-angle distribution for a 216-atom '*a*-Si model' from RMC simulations using experimental structure factor only. The approximate semi-circular distribution is a characteristic feature of *unconstrained* RMC.
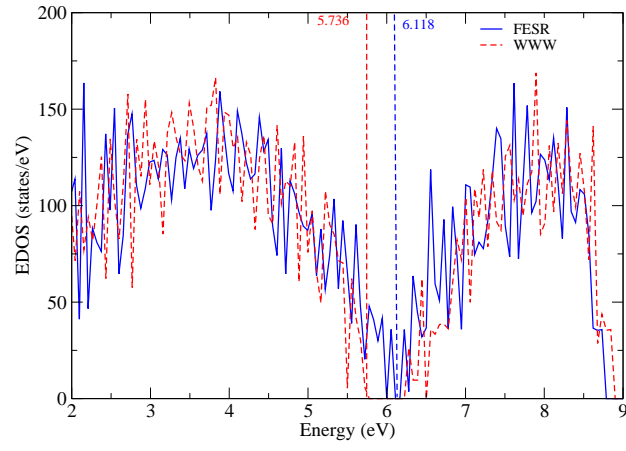
FIG. 12: (Color online) Density of electronic states of *a*-Si using VASP from FESR (blue) and WWW (red) models. The corresponding Fermi levels are indicated as vertical lines at 6.1 eV (FESR) and 5.7 eV (WWW).

Tables

TABLE I: Number of force calls and average CPU time in FESR compared with classical and quantum Melt-Quench method[25,26].

	192-atom	648-atom	1020-atom	1536-atom	CPMD (Ref[25])	Classical MD (Ref[26])
Number of force calls	3×10^4	3×10^4	3×10^4	3×10^4	27×10^4	6×10^4
CPU time (hours)	0.47	1.26	2.64	5.52		

TABLE II: Peak positions of FESR model compared with other MD models and experiments (Expt.).

Peak position (Å)			
atom-atom	FESR	MD (Ref[25])	Expt.(Ref[28])
Si-Si	3.15	3.10	
Si-O	1.62	1.62	1.610± 0.050
O-O	2.64	2.64	2.632± 0.089

TABLE III: Bond-angle distributions from FESR, MD and DR models.

Bond Angle (deg)			
	FESR	MD [25]	Expt. [30]	DR [6
O-Si-O	109.5 (15.6)	109.6 (10)	109.5	109.5 (9)
Si-O-Si	154.3 (27.8)	142.0 (25)	144 (38)	140 (25)

TABLE IV: Ring statistics of a-SiO$_2$ from FESR models.

Ring size (n)	4	6	8	10	12	14	16	18
192-atom	0	7	9	26	17	28	16	12
648-atom	5	12	36	57	80	109	53	42
1536-atom	6	24	108	167	195	215	148	96